PCCP

PAPER

View Article Online
View Journal | View Issue

Cite this: *Phys. Chem. Chem. Phys.*, 2014, **16**, 11303

Identifying sp–sp^2 carbon materials by Raman and infrared spectroscopies†

Jinying Wang,‡ Shuqing Zhang,‡ Jingyuan Zhou, Rong Liu, Ran Du, Hua Xu, Zhongfan Liu,* Jin Zhang* and Zhirong Liu*

Received 6th February 2014,
Accepted 23rd April 2014

DOI: 10.1039/c4cp00539b

www.rsc.org/pccp

Two-dimensional (2D) materials composed of sp and sp^2 carbon atoms (*e.g.*, graphyne and graphdiyne) show many interesting properties. These materials can be constructed through alkyne homocoupling; however, the occurrence of various side reactions increases the difficulty of their synthesis and structural characterization. Here, we investigate the thermodynamic properties and vibrational spectra of several arylalkynes. Both homocoupling and side reactions are found to occur spontaneously at room temperature in terms of thermodynamics. The calculated Raman spectra of the homocoupling products show regular changes with increasing polymerization degree. By rationalizing the vibrational modes of various oligomers, the Raman spectrum of a 2D sp–sp^2 carbon sheet is predicted; it exhibits three sharp peaks at 2241, 1560, and 1444 cm^{-1}. Although the target and byproducts display similar vibrational modes, a combination of Raman and infrared spectroscopies can be used to differentiate them. The theoretical results are then used to analyze the structure of a synthesized sample and provide useful information.

1. Introduction

Carbon forms various stable structures including diamond, graphite, fullerenes, carbon nanotubes (CNTs), and amorphous carbon materials. All of the existing and proposed carbon allotropes can be described as networks constructed from different combinations of sp^3-, sp^2- and sp-hybridized carbon atoms.[1] The discovery of graphene in 2004 and the numerous subsequent studies[2] have inspired the search for novel carbon allotropes.[3–8] Among the multifarious predicted carbon allotropes, the graphyne family,[9,10] which is a series of two-dimensional (2D) materials composed of sp and sp^2 carbon atoms, has received increasing attention because of the unique properties of its members.[4,11–16] These new carbon forms can behave as both metallic and semiconductive materials,[4,11] and Dirac cones have been found in some specific configurations.[12,16] Theoretical studies have shown that sp–sp^2 carbon materials could possess excellent mechanical properties.[13,15] Applications of sp–sp^2 carbon materials in electronic devices,[17] gas separation,[17–19] energy storage,[20–22] catalysis,[23,24] and solar cells[25] have been proposed.

Experimentally, the synthesis of infinite sp–sp^2 carbon materials is challenging and little success has been achieved. Initially, organic chemists obtained only oligomers.[26–28] In 2010, Li *et al.*[29] fabricated large graphdiyne films *via* a homocoupling reaction on copper surfaces, representing an encouraging step towards synthetic 2D polymers. Because of the lack of single or few-layer samples, structural characterization of the obtained graphdiyne films is also difficult. Recent experiments have indicated that several coupling reactions of ethynyl groups tend to occur simultaneously to form complex products.[30–33] Therefore, the efficient characterization of sp–sp^2 carbon materials is an important goal.

Vibrational spectroscopy (Raman and infrared (IR)) is a popular and convenient tool to characterize carbon materials.[34,35] Raman spectroscopy has been widely used to identify the layer number, defects and disorders, and doping levels of graphene,[36,37] as well as the diameter and chirality of CNTs.[38] Naturally, one may expect Raman spectroscopy to play an important role in the study of sp–sp^2 carbon materials. However, some basic vibrational properties of sp–sp^2 carbon materials remain unclear. For example, how do Raman spectra change with the degree of oligomerization? Can the homocoupling products be differentiated from others?

In this work, we conduct a theoretical and experimental study of the thermodynamic properties and vibrational spectra of several arylalkynes. This study has three objectives: to suggest how to promote the homocoupling of arylalkynes, to reveal how the Raman spectra of sp–sp^2 systems change with the degree of polymerization, and to demonstrate the usefulness of Raman and IR spectroscopies in identifying the various structures of these systems.

Center for Nanochemistry, College of Chemistry and Molecular Engineering, Peking University, Beijing 100871, PR China. E-mail: zfliu@pku.edu.cn, jinzhang@pku.edu.cn, LiuZhiRong@pku.edu.cn

† Electronic supplementary information (ESI) available: Theoretical and experimental methods, test calculations, and the Raman intensity of TEB oligomers. See DOI: 10.1039/c4cp00539b

‡ These authors contributed equally to this work.

2. Theoretical and experimental methods

2.1 Density functional theory calculations

All calculations were performed using density functional theory (DFT) using the Gaussian 03 package.[39] For the thermodynamic analysis, the hybrid functional B3LYP with the 6-311+G(d,p) basis set was used because of its good performance in thermochemistry.[40] Geometric optimizations were carried out at the same level. A test of the calculation method is provided in Table S1 in the ESI.† To calculate Raman and IR spectra, we chose the PBE functional and the 6-311+G(d,p) basis set after a series of tests (see Fig. S1 and S2 in the ESI†). The differences between the theoretical and experimental values of Raman peak positions for a few investigated compounds were less than 30 cm^{-1} in the range 1200–2400 cm^{-1}, confirming the reliability of the calculations. To reveal the general trends of the Raman spectra with increasing degree of oligomerization in sp–sp^2 carbon materials, the Raman spectra of some large systems were also calculated using the 6-31G(d) basis set and the PBE functional. The calculated vibrational frequencies were analyzed on the basis of potential energy distribution (PED) using the VEDA program,[41,42] which has been successfully used to analyze the distribution of vibrational energy previously.[43,44] With the help of VEDA, the assignment of bands was performed by internal coordinates.

2.2 Material synthesis and spectra measurements

Alkynes and solvents were obtained commercially and used without further purification. Copper foil was electrochemically polished in a phosphoric acid–glycol solution for 30 min, dried under a flow of nitrogen, and used immediately. 1,3,5-Triethynylbenzene (**1**, TEB, 0.015 g) was added to pyridine (100 mL) to prepare a solution with a concentration of 10^{-3} mol L^{-1}, and then a piece of copper foil (1 cm × 1 cm) was added to 10 mL of this solution. The mixture was stirred at 50 °C in an oil bath for 48 h. The copper foil was then washed sequentially with pyridine (20 mL) and dimethyl sulfoxide (20 mL) to remove monomers and oligomers. After drying the copper foil under a flow of nitrogen, a sp–sp^2 carbon film was obtained on the copper foil. Raman spectra were measured on a Horiba HR800 Raman spectrometer using a 632.8 nm excitation laser. Fourier transform IR spectra were recorded on a ThermoScientific Nicolet iN10 MX FT-IR spectrophotometer.

3. Results and discussion

3.1 Thermodynamic properties

We used compound **1** (TEB, Fig. 1a) as the monomer unit to construct the 2D sp–sp^2 carbon materials shown in Fig. 1c. When a homocoupling reaction occurs, a C–C covalent bond forms between two ethynyl groups, so the TEB monomer **1** is transformed into dimers **2**, trimers **3**, tetramers **4**, and other oligomers **4b**, **6**, **6b**, and **12** (Fig. 1a), and then may be eventually transformed into a 2D material (Fig. 1c). However, experiments in solution and under ultrahigh vacuum (UHV) have revealed that several types of side reactions can also occur, such as hydroalkynylation, trimerization, and oxidation,[30–32] leading to the random polymeric networks depicted in Fig. 1d. To investigate the various reaction pathways, we chose a simpler molecule **1′** (phenylacetylene, PA) as the reactant, from which molecules **2′–7′** were possible products (Fig. 1b).

We first examined the thermodynamic properties of the homocoupling and side reactions (Fig. 2). The change in standard enthalpy (ΔH_r) and Gibbs free energy (ΔG_r) for molecules in the gas phase were calculated by

$$\begin{aligned} \Delta H_r &= \sum H_{pr} - \sum H_{re} \\ \Delta G_r &= \sum G_{pr} - \sum G_{re}, \end{aligned} \quad (1)$$

where H_{pr} (G_{pr}) is the enthalpy (Gibbs free energy) of the product and H_{re} (G_{re}) is that of the reactant. ΔH_r and ΔG_r for the monomers (compounds **1** and **1′**) were set to 0. The specific reaction pathways are summarized in Fig. 2a. It should be noted that the homocoupling reactions might have two different pathways: (1) oxygen acts as an oxidant, which is the situation that usually occurs in solution; and (2) the C–C bonds form along with dehydrogenation (usually under UHV conditions).[31] Fig. 2b shows that all of the reactions are exothermic processes at room temperature. The difference between ΔH_r and ΔG_r is small, especially for the homocoupling reaction. For pathway (1) involving oxygen molecules (emphasized by red arrows in Fig. 2a), ΔH_r and ΔG_r (red symbols in Fig. 2b) are comparable with those of the side reactions (black symbols), and decrease with polymerization degree *n*. However, for pathway (2) including hydrogen generation (emphasized by blue arrows in Fig. 2a), the corresponding ΔH_r and ΔG_r (blue symbols in Fig. 2b) are very small (about −2 kcal mol^{-1}). This suggests that this type of reaction is relatively disadvantageous in thermodynamics. Previous studies have indicated that the substrates have the important effect of stabilizing 2D carbon materials. For example, the interaction between various metal substrates and graphene can decrease the energy of systems by 0.1–0.9 eV.[45] The novel sp–sp^2 carbon allotrope graphdiyne has also been synthesized on metal surfaces.[28] Therefore, the introduction of oxygen and selection of an appropriate metal substrate might increase the tendency to form the target 2D materials.

3.2 Raman spectra of oligomers

The above thermodynamic calculations suggest that homocoupling of alkynes should proceed exothermically. In experiments, it is difficult to identify the degree and direction of polymerization. The vibrations of a molecule are closely related to its structures, so we calculated the Raman spectra of the TEB monomer **1** and its oligomers to investigate how the Raman spectra change with polymerization (Fig. 3).

The calculation using the 6-311+G(d,p) basis set showed that the Raman spectrum of monomer **1** has three prominent peaks at 2146, 1566, and 1288 cm^{-1}, corresponding to A, G and D modes, respectively (Fig. 3a). The A mode is mainly contributed by C≡C stretching (C_{13} in Fig. $3b_1$), and the G mode mostly

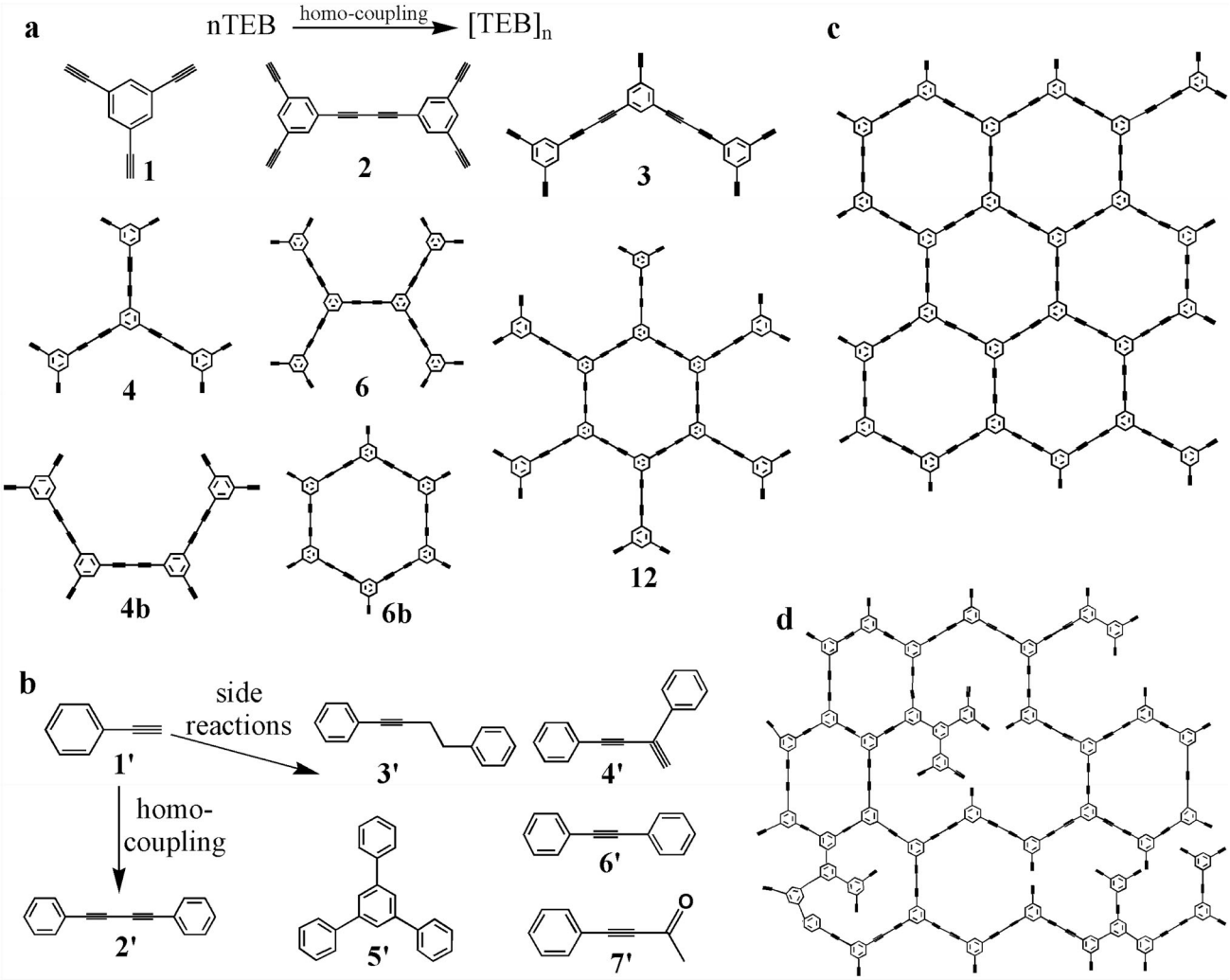

Fig. 1 Reaction schemes and products. (a) Homocoupling of **1** (TEB) to produce oligomers **2**, **3**, **4**, **4b**, **6**, **6b**, and **12**. (b) **1′** (phenylacetylene, PA) and its homocoupling product **2′** and various byproducts **3′–7′**. (c) The ideal 2D crystal of polymerized **1**. (d) A hypothetical network with irregular crosslinking of **1**.

comes from C=C aromatic stretching (C_{12} in Fig. $3b_1$), while the stretching of the C–C bonds (C_{11} in Fig. $3b_1$) between triply-coordinated atoms and its doubly-coordinated neighbors makes the largest contribution to the D mode. Once the homocoupling reaction occurs, a sharp peak at 2241 cm^{-1} (A′ mode) appears, which is attributed to the stretching vibration of the conjugated diyne groups; *i.e.*, synchronous stretching of two adjacent acetylene bonds (C_{23} in Fig. $3b_2$). In contrast, the stretching of the bonds between two carbon triple bonds (C_{22} in Fig. $3b_2$) coupled with that of the C–C bonds between triply-coordinated atoms and its doubly-coordinated neighbors (C_{21} in Fig. $3b_2$) contributed to the new vibrational D′ mode (Fig. 3a and b_2). The peak intensities of the A, A′, G, and D′ modes gradually increase with polymerization degree n (see Fig. S4 in the ESI†), but the peak positions shift in different directions. The frequencies of the A and A′ modes remain constant because the vibrations tend to be localized near the triple carbon bonds. The G vibration changes little, except for in the Raman spectrum of compound **4**, which shows a shoulder peak at 1552 cm^{-1} mainly from the extended C=C bonds of the central phenyl rings. However, the frequency of the D′ vibration exhibits a blue shift from 1433 to 1435 to 1440 cm^{-1} for compounds **2**, **3**, and **4** with increasing n.

To better understand the variation of the Raman spectra with the polymerization degree for the systems based on **1**, we calculated the Raman spectra of more oligomers (compounds **1–4**, **4b**, **6**, **6b**, and **12**) using the smaller 6-31G(d) basis set (Fig. 3c). Although the Raman peak positions calculated using the 6-31G(d) basis set are not as accurate as those determined using the 6-311+G(d,p) basis set, the variation of trends of both the Raman peak position and intensity with n is consistent for both basis sets (see Table S2 and Fig. S4 in the ESI†). As shown in Fig. S4 (ESI†), the peak intensities of the A, A′, G, and D′ modes increase monotonically with n for the systems we examined. In particular, the intensity ratio of A′ to A (A′/A) linearly increases with n, while the ratio of D′ to G (D′/G) starts to converge at large n (Fig. 3d). The Raman peak positions of A′ and A are constant, as discussed above, while those of G and D′

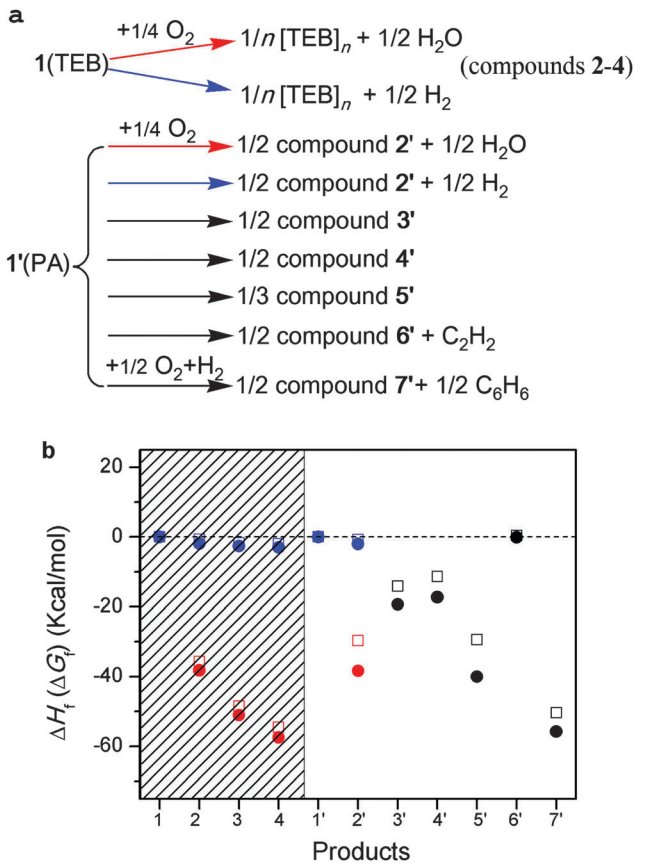

Fig. 2 Reaction pathways and thermodynamic analysis. (a) Pathways of homocoupling with oxygen participating (red arrows), dehydrogenation (blue arrows), and side reactions (black arrows). $[TEB]_n$ denotes the homocoupling products of TEB with polymerization degree n. (b) The changes of standard enthalpy ΔH_r are shown as solid circles and the Gibbs free energy ΔG_r as open squares. Red is used for the oxidative homocoupling pathway, blue for the pathway with dehydrogenation, and black for the side reactions.

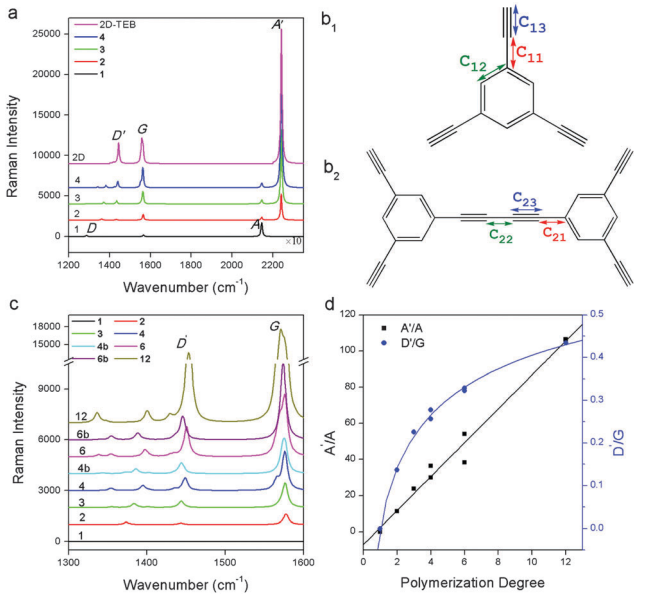

Fig. 3 Calculated Raman spectra of the TEB monomer **1** and its oligomers, the intensity of peaks are expressed by the calculated amplitude. (a) Raman spectra of monomer **1** (the intensity has been amplified by 10), homocoupling oligomers **2**, **3**, and **4**, and the 2D TEB sheet. (b_1) Monomer **1**, where C_{11}, C_{12}, and C_{13} represent the bonds between triply-coordinated atoms and its doubly-coordinated neighbors, the bonds of aromatic rings, and the bonds of carbon triple bonds in the TEB monomer, respectively. (b_2) Dimer **2**, where C_{21}, C_{22}, C_{23} represent bonds between a triply-coordinated atoms and its doubly-coordinated neighbors, the single bonds between two triple carbon bonds, and the carbon triple bonds in the TEB dimer, respectively. (c) Raman spectra of the systems **1–4**, **4b**, **6**, **6b**, and **12** calculated using the 6-31G(d) basis set. (d) Raman intensity ratios of A′ to A (A′/A, black squares) and of D′ to G (D′/G, blue circles).

depend on both the degree and direction of polymerization (Fig. 3c). The changes of the Raman peak positions gradually decrease with increasing n. For example, the Raman peak positions of the G mode are the same for molecules **6** and **12** and those of the D′ mode differ by only 2 cm^{-1}. The oligomers showed more vibration modes in the range from 1200 to 1400 cm^{-1}, but the intensities are relatively low.

3.3 Raman spectra of 2D materials

Based on the above analyses, we attempted to predict the Raman spectrum of 2D TEB sheets using a recursive method[46] and rationalizing the vibrational modes. The A′ and A vibrations are characteristic of alkynes. The A′ mode is mostly attributed to the stretching vibration of the conjugated diyne groups and shows strong Raman activity at 2241 cm^{-1} for all of the oligomers, so this peak is also expected to be present in the Raman spectrum of a 2D TEB sheet. In contrast, the A mode mainly comes from the vibration of the ethynyl groups and would not be present in the Raman spectrum of the 2D TEB sheet. This is also consistent with the above observation that A′/A increases with n (Fig. 3d).

The intensity of the G mode indicates the number of phenyl rings, and that the peak position is not affected much by the linked groups. Therefore, the 2D TEB sheet is expected to possess a Raman peak near 1560 cm^{-1} from the G mode. The D′ mode is mostly influenced by the stretching of the bonds between two carbon triple bonds (C_{22} in Fig. $3b_2$), which is Raman active because of the molecule's D2H symmetry. Moreover, the ratio of the intensity of D′ to G modes (D′/G) tends to converge for TEB oligomers at large n (Fig. 3d) and the peak position of D′ approaches 1444 cm^{-1}. Other Raman peaks were temporarily ignored because they show low Raman activity in oligomers. Overall, the speculated Raman spectrum of the ideal 2D TEB network has three strong peaks at 2241 (A′), 1560 (G), and 1444 cm^{-1} (D′), as shown in Fig. 3a.

Notably, the vibrations of the above speculated Raman peaks (A′, G, and D′) for 2D TEB (Fig. 3a) all occur at the Γ point in reciprocal space. The conservation of momentum is satisfied in the Raman response without the involvement of any defects. Thus, these are intrinsic Raman peaks of 2D TEB. This is different from the case of graphene where the ring-breathing mode (D) occurs at the K point and is inhibited without defects (so the D peak in graphene acts as an indicator of the content of defects). However, above speculated peaks in 2D TEB cannot be used to characterize defect content. Graphdiyne may possess similar Raman features to 2D TEB.

3.4 Combination of Raman and IR spectroscopies

Besides the homocoupling products, many side reactions could also occur in the systems of **1** and **1′**. To differentiate the various functional groups, we calculated the Raman spectra of compounds **1′**–**7′** (Fig. 4a). The most obvious change in the Raman spectrum of **1′** after homocoupling is the appearance of the strong Raman-active vibration A′, which is similar to that of TEB. Unexpectedly, the byproducts also have Raman peaks around 2220 cm^{-1} except for compound **5′**. The relative Raman positions of the C≡C stretching peak for compounds **3′**, **4′**, **6′**, and **7′** compared with the corresponding peak of **2′** are −27, −9, −5, and −20 cm^{-1}, respectively. The aromatic ring stretching peak also shows Raman activity for all of the products, and the largest difference between the peak position of the byproducts and the corresponding peak of **2′** is −8 cm^{-1}. Although the D′ vibration is unique for the homocoupling products, another peak exists near its Raman peak for compound **3′**. In addition, compounds **3′** and **5′** both have a coupled C–H vibration and a ring breathing peak at 1298 and 1310 cm^{-1}, respectively, which is not present in the other compounds. Byproduct **7′** also has a unique C=O stretching vibration at 1656 cm^{-1}, although its Raman intensity is very low so it is difficult to detect. Overall, the functional groups of compounds **4′**, **6′**, and **7′** are difficult to distinguish in Raman spectra, whereas the functional groups of compounds **3′** and **5′** are relatively easy to distinguish.

Because it is difficult to use Raman spectroscopy to identify all of the functional groups introduced by the side reactions, we also used IR spectroscopy to examine the systems, which also shows molecular vibrations but usually provides complementary information to Raman spectroscopy. The calculated results are summarized in Fig. 4b. Compound **7′** is the easiest to identify because of the strong IR activity of the C=O stretching peak at 1655 cm^{-1} and the C≡C stretching peak at 2216 cm^{-1}. If the analogues of **7′** are ruled out from the system, similar structures of **4′** and **5′** can be confirmed by their IR peaks near 1330 and 1401 cm^{-1}, respectively. The IR spectra of **6′** and **2′** show similar peak shape, but the former has a peak at 1467 cm^{-1} while the latter has one at 1489 cm^{-1}. Products **2′** and **3′** cannot be differentiated from IR spectra alone. However, we can identify almost all of the types of byproducts by combining Raman and IR spectroscopies.

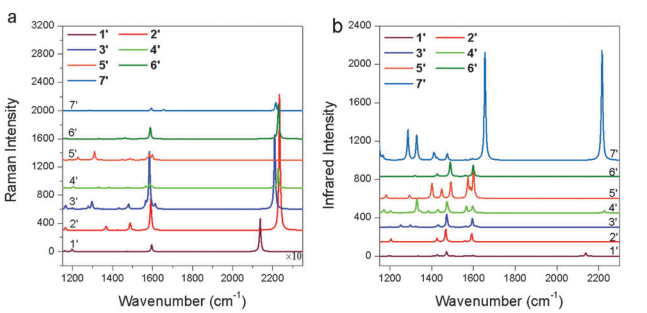

Fig. 4 Calculated (a) Raman and (b) IR spectra for molecules **1′**–**7′**. The Raman intensity of molecule **1′** was amplified 10 times.

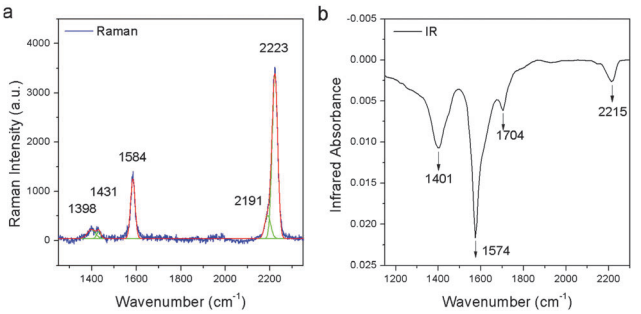

Fig. 5 (a) Raman and (b) IR spectra of a typical experimental sample. Raman spectra are fitted by five Gaussian functions after baseline corrections.

3.5 Structural analysis of the experimental sample

The insights obtained from the calculations are useful for analyzing experimental results. Fig. 5a shows a typical Raman spectrum of the product synthesized using monomer **1** as the reactant. The disappearance of the peak at ~2100 cm^{-1} indicates that **1** has reacted. The two peaks at 1398 and 1431 cm^{-1} are consistent with the calculated Raman peaks of oligomers of **1**, but it is also possible that they belong to a large variety of saturated hydrocarbons. The peaks at 2223 and 2191 cm^{-1} suggest the formation of both the targeted product and byproducts. Because the position difference of the two peaks near 2200 cm^{-1} is greater than 30 cm^{-1}, the functional groups of molecule **3′** might exist in the product. However, we did not observe a peak near 1310 cm^{-1}, which characterizes the formation of molecule **3′**, because of the fluctuation of the baseline. This also leads to difficulty in identifying other byproducts. Generally, a carbon material with amorphous structure displays much broader Raman peaks compared with that of a crystalline sample. In Fig. 5a, the peaks are sharp, suggesting that little or no amorphous structure is formed. Interestingly, by analyzing the Raman spectra obtained for our synthesized films and those reported in the literature,[29] we did not observe any high-order (multiphonon) Raman peaks as found for graphene,[47] which may suggest that high-order Raman resonant processes are not important in 2D TEB and other sp–sp^2 carbon materials. We also measured the IR spectra of the sample (Fig. 5b). Two strong IR peaks at ~1704 and ~2215 cm^{-1} indicate that maybe there exists some analogue of compound **7′**. The peaks near 1574 and 1401 cm^{-1} are broad and the superimposition of multiple peaks indicates a similar structure to **5′**. Although it is currently difficult to identify the structures present in the experimental sample, the calculation analysis provides criteria to identify the degree of polymerization and functional groups in sp–sp^2 carbon materials.

4. Conclusions

In summary, we used Raman and IR spectroscopies to identify the structure of sp–sp^2 carbon materials. After demonstrating that many coupling reactions of alkynes can occur spontaneously at room temperature, we conducted a combined computational and experimental study of the vibration spectra of several alkynes. Regular changes of the Raman spectra were observed

with increasing homocoupling polymerization degree. The three Raman-active modes, A′ ($\sim$2240 cm^{-1}), G ($\sim$1565 cm^{-1}), and D′ ($\sim$1440 cm^{-1}), were found to be important for identifying the degree of polymerization. By rationalizing the vibrational modes of various oligomers, we predicted the Raman spectrum of the 2D-TEB network. The combination of Raman and IR spectra is useful for identifying the functional groups in sp–sp^2 carbon materials. Based on this, we examined the structure of an experimental sample.

Acknowledgements

We thank Shibin Deng and Zhenzhu Li for valuable discussion. This work was supported by the National Natural Science Foundation of China (Grant No. 21373015, 51121091, and 51290272), the Ministry of Science and Technology of China (Grant No. 2013CB932603, 2012CB933404, and 2011CB933003), and the Overseas and Hong Kong, Macao Young Scholars Collaborative Research Fund (Grant No. 21129001).

Notes and references

1 R. B. Heimann, S. E. Evsyukov and Y. Koga, *Carbon*, 1997, **35**, 1654–1658.
2 K. S. Novoselov, A. K. Geim, S. V. Morozov, D. Jiang, Y. Zhang, S. V. Dubonos, I. V. Grigorieva and A. A. Firsov, *Science*, 2004, **306**, 666–669.
3 A. Hirsch, *Nat. Mater.*, 2010, **9**, 868–871.
4 A. N. Enyashin and A. L. Ivanovskii, *Phys. Status Solidi B*, 2011, **248**, 1879–1883.
5 J. Y. Wang, H. Q. Huang, W. H. Duan and Z. R. Liu, *J. Chem. Phys.*, 2013, **139**, 184701.
6 X.-L. Sheng, Q.-B. Yan, F. Ye, Q.-R. Zheng and G. Su, *Phys. Rev. Lett.*, 2011, **106**, 155703.
7 S. Nardecchia, D. Carriazo, M. L. Ferrer, M. C. Gutierrez and F. del Monte, *Chem. Soc. Rev.*, 2013, **42**, 794–830.
8 Z. R. Liu, J. Y. Wang and J. L. Li, *Phys. Chem. Chem. Phys.*, 2013, **15**, 18855–18862.
9 R. H. Baughman, H. Eckhardt and M. Kertesz, *J. Chem. Phys.*, 1987, **87**, 6687–6699.
10 A. L. Ivanovskii, *Prog. Solid State Chem.*, 2013, **41**, 1–19.
11 N. Narita, S. Nagai, S. Suzuki and K. Nakao, *Phys. Rev. B: Condens. Matter Mater. Phys.*, 1998, **58**, 11009–11014.
12 D. Malko, C. Neiss, F. Vines and A. Gorling, *Phys. Rev. Lett.*, 2012, **108**, 086804.
13 S. W. Cranford and M. J. Buehler, *Carbon*, 2011, **49**, 4111–4121.
14 J. Kang, J. B. Li, F. M. Wu, S. S. Li and J. B. Xia, *J. Phys. Chem. C*, 2011, **115**, 20466–20470.
15 Y. Y. Zhang, Q. X. Pei and C. M. Wang, *Appl. Phys. Lett.*, 2012, **101**, 081909.
16 H. Q. Huang, W. H. Duan and Z. R. Liu, *New J. Phys.*, 2013, **15**, 023004.
17 Y. Jiao, A. Du, M. Hankel, Z. Zhu, V. Rudolph and S. C. Smith, *Chem. Commun.*, 2011, **47**, 11843–11845.
18 S. W. Cranford and M. J. Buehler, *Nanoscale*, 2012, **4**, 4587–4593.
19 H. Y. Zhang, X. J. He, M. W. Zhao, M. Zhang, L. X. Zhao, X. J. Feng and Y. H. Luo, *J. Phys. Chem. C*, 2012, **116**, 16634–16638.
20 Y. H. Guo, K. Jiang, B. Xu, Y. D. Xia, J. Yin and Z. G. Liu, *J. Phys. Chem. C*, 2012, **116**, 13837–13841.
21 H. J. Hwang, J. Koo, M. Park, N. Park, Y. Kwon and H. Lee, *J. Phys. Chem. C*, 2013, **117**, 6919–6923.
22 H. Y. Zhang, Y. Y. Xia, H. X. Bu, X. P. Wang, M. Zhang, Y. H. Luo and M. W. Zhao, *J. Appl. Phys.*, 2013, **113**, 044309.
23 N. L. Yang, Y. Y. Liu, H. Wen, Z. Y. Tang, H. J. Zhao, Y. L. Li and D. Wang, *ACS Nano*, 2013, **7**, 1504–1512.
24 S. Wang, L. Yi, J. E. Halpert, X. Lai, Y. Liu, H. Cao, R. Yu, D. Wang and Y. Li, *Small*, 2012, **8**, 265–271.
25 H. Du, Z. Deng, Z. Lü, Y. Yin, L. Yu, H. Wu, Z. Chen, Y. Zou, Y. Wang, H. Liu and Y. Li, *Synth. Met.*, 2011, **161**, 2055–2057.
26 M. M. Haley, *Pure Appl. Chem.*, 2008, **80**, 519–532.
27 J. Sakamoto, J. van Heijst, O. Lukin and A. D. Schluter, *Angew. Chem., Int. Ed.*, 2009, **48**, 1030–1069.
28 F. Diederich and M. Kivala, *Adv. Mater.*, 2010, **22**, 803–812.
29 G. X. Li, Y. L. Li, H. B. Liu, Y. B. Guo, Y. J. Li and D. B. Zhu, *Chem. Commun.*, 2010, **46**, 3256–3258.
30 Y. Q. Zhang, N. Kepcija, M. Kleinschrodt, K. Diller, S. Fischer, A. C. Papageorgiou, F. Allegretti, J. Bjork, S. Klyatskaya, F. Klappenberger, M. Ruben and J. V. Barth, *Nat. Commun.*, 2012, **3**, 1286.
31 J. Eichhorn, W. M. Heckl and M. Lackinger, *Chem. Commun.*, 2013, **49**, 2900–2902.
32 H.-Y. Gao, J.-H. Franke, H. Wagner, D. Zhong, P.-A. Held, A. Studer and H. Fuchs, *J. Phys. Chem. C*, 2013, **117**, 18595–18602.
33 H.-Y. Gao, H. Wagner, D. Y. Zhong, J.-H. Franke, A. Studer and H. Fuchs, *Angew. Chem., Int. Ed.*, 2013, **52**, 4024–4028.
34 *Raman Spectroscopy in Carbons: from Nanotubes to Diamond*, ed. A. C. Ferrari and J. Robertson, 2004.
35 E. Fuente, J. A. Menéndez, M. A. Díez, D. Suárez and M. A. Montes-Morán, *J. Phys. Chem. B*, 2003, **107**, 6350–6359.
36 A. C. Ferrari, J. C. Meyer, V. Scardaci, C. Casiraghi, M. Lazzeri, F. Mauri, S. Piscanec, D. Jiang, K. S. Novoselov, S. Roth and A. K. Geim, *Phys. Rev. Lett.*, 2006, **97**, 187401.
37 L. M. Malard, M. A. Pimenta, G. Dresselhaus and M. S. Dresselhaus, *Phys. Rep.*, 2009, **473**, 51–87.
38 A. Jorio, R. Saito, J. H. Hafner, C. M. Lieber, M. Hunter, T. McClure, G. Dresselhaus and M. S. Dresselhaus, *Phys. Rev. Lett.*, 2001, **86**, 1118–1121.
39 M. J. Frisch, G. W. Trucks, H. B. Schlegel, G. E. Scuseria, M. A. Robb, J. R. Cheeseman, J. A. Montgomery, Jr., T. Vreven, K. N. Kudin, J. C. Burant, J. M. Millam, S. S. Iyengar, J. Tomasi, V. Barone, B. Mennucci, M. Cossi, G. Scalmani, N. Rega, G. A. Petersson, H. Nakatsuji, M. Hada, M. Ehara, K. Toyota, R. Fukuda, J. Hasegawa, M. Ishida, T. Nakajima, Y. Honda, O. Kitao, H. Nakai, M. Klene, X. Li, J. E. Knox, H. P. Hratchian, J. B. Cross, V. Bakken, C. Adamo, J. Jaramillo, R. Gomperts, R. E. Stratmann, O. Yazyev, A. J. Austin, R. Cammi, C. Pomelli, J. W. Ochterski,

P. Y. Ayala, K. Morokuma, G. A. Voth, P. Salvador, J. J. Dannenberg, V. G. Zakrzewski, S. Dapprich, A. D. Daniels, M. C. Strain, O. Farkas, D. K. Malick, A. D. Rabuck, K. Raghavachari, J. B. Foresman, J. V. Ortiz, Q. Cui, A. G. Baboul, S. Clifford, J. Cioslowski, B. B. Stefanov, G. Liu, A. Liashenko, P. Piskorz, I. Komaromi, R. L. Martin, D. J. Fox, T. Keith, M. A. Al-Laham, C. Y. Peng, A. Nanayakkara, M. Challacombe, P. M. W. Gill, B. Johnson, W. Chen, M. W. Wong, C. Gonzalez and J. A. Pople, *Gaussian 03*, Gaussian, Inc, Wallingford CT, 2004.

40 X. Xu and W. A. Goddard, *J. Chem. Phys.*, 2004, **121**, 4068–4082.

41 M. H. Jamróz, *Vibrational Energy Distribution Analysis VEDA 4*, Warsaw, 2004.

42 M. H. Jamróz, *Spectrochim. Acta, Part A*, 2013, **114**, 220–230.

43 S. Ostrowski, M. H. Jamroz, J. E. Rode and J. C. Dobrowolski, *J. Phys. Chem. A*, 2012, **116**, 631–643.

44 J. R. Maia, J. A. Lima Jr., P. T. C. Freire, J. Mendes Filho, C. E. S. Nogueira, A. M. R. Teixeira, A. S. de Menezes, C. M. R. Remédios and L. P. Cardoso, *J. Mol. Struct.*, 2013, **1054–1055**, 143–149.

45 P. Sutter, M. S. Hybertsen, J. T. Sadowski and E. Sutter, *Nano Lett.*, 2009, **9**, 2654–2660.

46 C. Castiglioni, F. Negri, M. Rigolio and G. Zerbi, *J. Chem. Phys.*, 2001, **115**, 3769–3778.

47 D. M. Basko, *Phys. Rev. B: Condens. Matter Mater. Phys.*, 2008, **78**, 125418.